ingegneria sismica
International Journal of Earthquake Engineering
Anno XLIII - Num. 1 - 2026

Mechanical Error Analysis and Compensation Techniques in High-Precision Measurement of Moment of Inertia

Yang Su[1], *Hang Xiu*[2], *Lifang Wang*[1], *Lei Cheng*[1] *and Qi Qin*[3,*]

[1] Chongqing Academy of Metrology and Quality Inspection, Chongqing, 401123, China
[2] Chongqing Research Institute, Changchun University of Science and Technology, Chongqing, 401135, China
[3] Chongqing Institute of Engineering, Chongqing, 4000056, China

SUMMARY: *CNC machine tools and relevant machines have been widely used in various fields, including aerospace, instrument making, medicine, mold processing, etc., wherein machining accuracy will affect the final performance of products. In this paper, firstly, the torsion pendulum method for measuring rotational inertia is introduced, and an accurate measurement device is designed based on the physical principle. Next, by applying the Hilbert transform, a novel time-frequency analysis technique is adopted to discover the mathematical formula of the relationship between the rotational inertia of the test object and its undamped natural frequency. Therefore, a computational method of rotational inertia utilizing Hilbert transform is constructed. Lastly, MATLAB simulation and experiments based on the least squares estimation are conducted to validate the effect of the mechanical compensation method for measuring rotational inertia with the help of Hilbert transform. Experimental results demonstrate that the relative error of the computational algorithm proposed in this paper is less than 0.5%, outperforming the traditional periodic algorithm. Moreover, the temperature compensation algorithm makes a significant contribution to enhancing the accuracy of rotational inertia measurement with varying temperature of the torsion bar.*

KEYWORDS: *rotational inertia; Hilbert transform; torsion pendulum method; least squares method*

1 Introduction

The measurement of the moment of inertia of a rigid body is of considerable importance, and it is also a key parameter in scientific research, engineering applications, aerospace, electric-power systems, machinery, instrumentation, and other industrial sectors [1, 2]. For a rigid body with a regular geometry, the moment of inertia can usually be obtained directly through analytical formulas, whereas that of an irregular or non-uniform rigid body is more often identified by experimental approaches [3-5]. For example, Zhang et al [6] developed a deviation-based approach for measuring rotational inertia using the torsion-bar method. After examining sources of measurement error, positioning error, and damping, they showed that the measurement precision could be controlled within 0.1% under ideal conditions. Thomson [7] adopted an experimental approach based on a three-wire pendulum to determine the period and combined it with the principle of mechanical energy conservation, thereby providing a relatively straightforward method for evaluating the rotational inertia of irregular three-

*qinqi1008@163.com
https://doi.org/10.65102/is2026194
Published: 30 April, 2026

dimensional mass-imbalanced objects. This method has the advantages of simplicity and high accuracy for the measurement of rotational inertia of irregular and uneven mass objects. The basic methods for the experimental determination of the moment of inertia of a rigid body include the torsional pendulum method and the three-linear pendulum method, but the above methods often have different degrees of defects that affect the accuracy of the measurement results. With the demand for micrometer-level accuracy in aerospace and mechanical engineering, the traditional rotational inertia measurement methods have been difficult to meet. Based on this, it is of great significance to carry out high-precision rotational inertia measurement and study different error factors and compensation techniques in rotational inertia measurement applications.

Morelli [8] constructed a dynamic model based on the equation error of the flight test state and the controlled data to determine the rotational inertia of an aircraft, and found that the method can control the measurement error within 6% under nonlinear simulation.Tang et al [9] developed an extended disturbance observer in combination with a triggering mechanism for the estimation of line-load torque and rotational inertia, which is able to achieve system load anti-interference performance, reduce the tracking error, and have utility in the high-precision identification of complex industrial equipment. Chen et al [10] have modeled torsional vibration with linear damping. The model was utilized to determine angular displacement through analyzed photographs in order to obtain the vibration period and amplitude modulation factor, which then helped find the accurate moment of inertia of the load. In addition, Wang [11] constructed a dynamic model for rotational inertia measurement, this type of mathematical model is feasible, but its measurement accuracy will be affected by the uncertainty of the instrument and the model error, and the maximum error is as high as 39%. Jung [12] used the neural network technology to formulate the intelligent method for compensating the inertial model error in the time-lag controller used for robot manipulators, which is able to compensate for the inertia matrix's constant deviation to improve the robot operating performance and maintain the boundary stability. Zhou et al [13] proposed a real-time compensation of dynamic load position error in a dual-inertia drive system based on mechanical parameter prediction without the need of position sensor mounting, which controls the load position error to almost zero. The rotational inertia measurement has gradually shifted from traditional methods such as torsion pendulum method and three-line pendulum method to intelligent methods, and the compensation technique has gradually reduced the error to below 0.1%. However, the complexity of the measurement process, cost and accuracy breakthrough is still the focus of the current measurement technology considerations.

Firstly, a highly accurate model for rotational inertia measurement is presented, and the structure and working mechanism of the measuring apparatus are explained. Next, the correlation between rotational inertia and instantaneous undamped natural frequency of the vibration system in torsion pendulum oscillation is studied, and then the calculation process of rotational inertia through Hilbert transform is discussed. Then numerical simulations and error analysis of experimental measurements are carried out in order to prove the feasibility of Hilbert transform-based method for the estimation of rotational inertia. Lastly, a temperature compensation scheme for rotational inertia measurement is obtained via least square method, and its effectiveness is verified by experiments.

2 High-precision rotational inertia measurement models

2.1 Measurement of the moment of inertia

Depending on the state of the object to be measured at the time of measurement, there are two types of measurement of rotational inertia: on-line measurement and off-line measurement. On-line measurement refers to the measurement when the measured part is in working condition, and off-line measurement is just the opposite. The devices that use on-line measurement are engines, internal combustion engines and generators. Generally speaking, the accuracy of on-line measurement is limited, the relative error of measurement is about 2%, the reason why this method is used is because the complexity of the measured part is not possible to apply off-line measurement or the application of off-line measurement of the results obtained and the actual rotational inertia of the measured part of the work of a larger deviation. Compared with on-line measurement, off-line measurement has high accuracy and is more widely used. Offline measurement methods mainly include compound pendulum equivalence method, falling body method, linear pendulum method, torsion pendulum method. There are also some special measurement methods, such as the measurement of the moment of inertia of automobile based on the vibration principle, which are also categorized as offline measurement.

2.2 Basic principle of rotational inertia measurement by torsion pendulum method

As a high sensitivity detection tool, precision torsion pendulum has been widely used in many fields such as precision measurement of weak forces such as gravitational force and electromagnetic force, as well as material characterization. The upper end of the torsion bar is fixed, and the lower end is connected to the disk, the rotational inertia of the disk is J, the swing angle is θ, and the stiffness coefficient of the torsion bar K is considered to be a constant when the swing angle is very small. Apply a certain torque on the disk, the disk will rotate by an angle, when the external torque is suddenly withdrawn, the torsion bar will drive the disk for simple harmonic vibration. Neglecting the mass and moment of inertia of the torsion bar, the free vibration equation of the torsion pendulum can be expressed as:

$$J\ddot{\theta} + R\dot{\theta} + K\theta = 0 \tag{1}$$

where R denotes the equivalent damping coefficient. Let f denote the undamped self-oscillation frequency of the torsional pendulum and ξ denote the damping ratio, the solution of Eq. (1) can be expressed as:

$$\theta(t) = A\exp(-2\pi\xi f)\cos\left(2\pi f\sqrt{1-\xi^2}t + \varpi\right) \tag{2}$$

where A and ϖ are constants determined by the initial conditions, and $f\sqrt{1-\xi^2}$ denotes the damped self-oscillation frequency of the system.

2.3 Structure of high-precision rotational inertia measuring instrument

A high-precision rotational inertia measuring instrument used to measure the rotational inertia of an aircraft has been designed as an inverted torsion pendulum. A cross-sectional view of the instrument is given in Figure 1. The stability of the rotational center of the measuring stage is ensured by radial bearings, thrust bearings are used to carry the measured parts and tooling, a

cylinder provides the initial excitation force, and the free decay response of the torsion pendulum is captured by a laser displacement sensor. When the thrust bearings are inflated into operation, the measuring table floats upwards by a few tens of microns, and a flexible coupling is used to overcome this displacement.

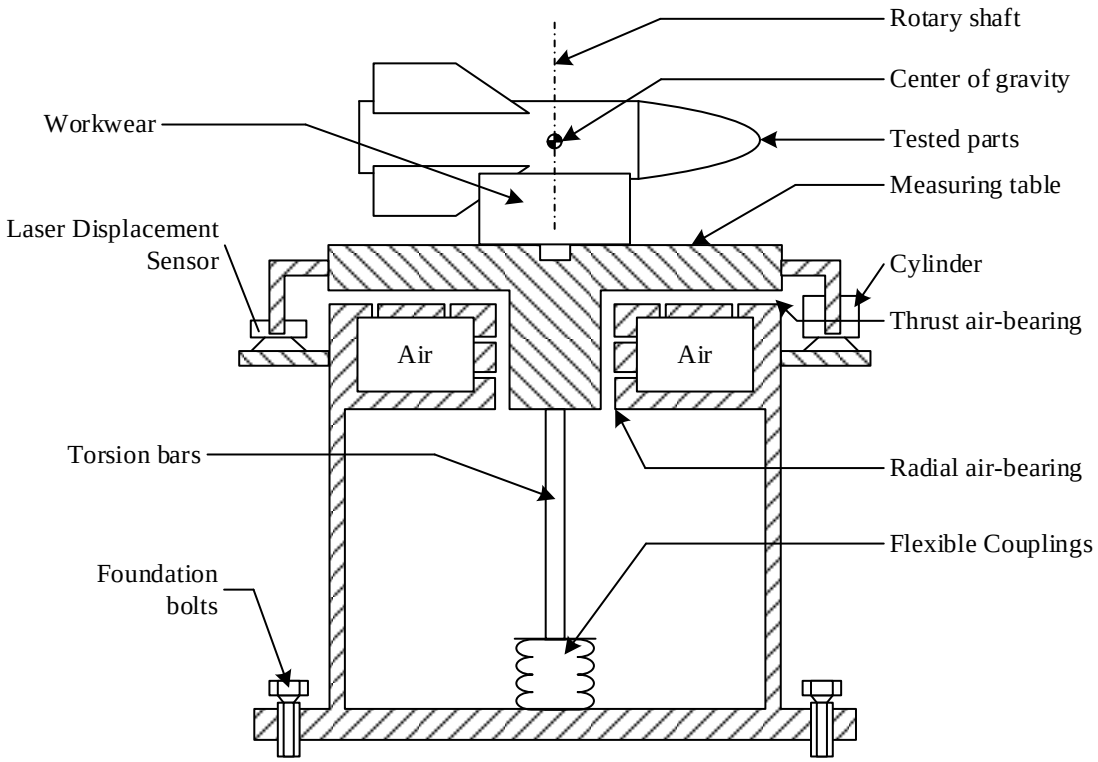

Figure 1: Cutaway view of instrument used to measure MOI

The instrument mainly adopts the following two technical means to ensure the measurement accuracy:

1. Hydrostatic gas bearing

Whether the bearing can provide high-precision and small-damping support for the rotational inertia measurement system is the key to determine the accuracy of the rotational inertia measurement results. Gas bearings are mechanical components that utilize gas film to support load or reduce friction. Considering that gas bearings have many advantages such as low frictional resistance, smooth operation, high precision, no crawling in low-speed movement, low vibration and low wear, etc., hydrostatic gas bearings are used to ensure the rotary accuracy and support the rigid connecting body composed of rotary table, workpiece and the measured parts in the instrument.

2. High-precision laser displacement sensor

The traditional rotational inertia measurement equipment is often used in the photoelectric timing method to directly obtain the vibration cycle of the torsion pendulum, but this method of photoelectric switch installation position of high precision requirements. Instrument selection of German Micro-Epsilon production of high-precision laser displacement sensor optoNCDT1700 (range 20mm, linearity ± 0.08%) on the turntable deviation from the balance position of the straight-line distance of non-contact precision measurement, and then through the system identification method to estimate the system's undamped self-oscillation frequency and damping ratio.

3 High-precision rotational inertia calculation method

3.1 Calculation method of rotational inertia based on Hilbert transformation

3.1.1 Construction of parsed signals

If $\theta(t)$ is a continuous real-valued signal, then the Hilbert transform of $\theta(t)$ is defined as:

$$\tilde{\theta}(t) = H[\theta(t)] = \frac{1}{\pi}\int_{-\infty}^{+\infty}\frac{\theta(\tau)}{t-\tau}\mathrm{d}\tau \tag{3}$$

If $\theta(t)$ is a real-valued signal and $\tilde{\theta}(t)$ is the Hilbert transform of $\theta(t)$, then the analytic signal corresponding to $\theta(t)$ is:

$$\boldsymbol{\beta} = \theta(t) + j\tilde{\theta}(t) = A(t)e^{j\varphi(t)} \tag{4}$$

where $\boldsymbol{\beta}$ is the resolved signal, $A(t)$ is the instantaneous amplitude, and $\varphi(t)$ is the instantaneous phase.

The expressions for $A(t)$ and $\varphi(t)$ can be obtained from equation (4):

$$A(t) = \sqrt{\theta^2(t) + \tilde{\theta}^2(t)} \tag{5}$$

$$\varphi(t) = \arctan\left[\frac{\tilde{\theta}(t)}{\theta(t)}\right] \tag{6}$$

The instantaneous angular frequency $\omega(t)$ is defined as the first order derivative of the instantaneous phase:

$$\omega(t) = \frac{d\varphi}{dt} \tag{7}$$

Taking one derivative of the analytic signal $\boldsymbol{\beta}$ with respect to t gives:

$$\dot{\boldsymbol{\beta}} = \boldsymbol{\beta}\left[\frac{\dot{A}(t)}{A(t)} + j\omega(t)\right] \tag{8}$$

The formula for the instantaneous angular frequency can be obtained from equation (8):

$$\omega(t) = \mathrm{Im}\left[\frac{\dot{\boldsymbol{\beta}}(t)}{\boldsymbol{\beta}(t)}\right] = \frac{\theta(t)\dot{\tilde{\theta}}(t) - \dot{\theta}(t)\tilde{\theta}(t)}{\theta^2(t) + \tilde{\theta}^2(t)} \tag{9}$$

The formula for the first order derivative of the instantaneous amplitude can be obtained from equation (9):

$$\dot{A}(t) = A(t)\,\mathrm{Re}\left[\frac{\dot{\boldsymbol{\beta}}(t)}{\boldsymbol{\beta}(t)}\right] = \frac{\theta(t)\dot{\theta}(t) + \tilde{\theta}(t)\dot{\tilde{\theta}}(t)}{\sqrt{\theta^2(t) + \tilde{\theta}^2(t)}} \tag{10}$$

3.1.2 Discrete Hilbert transforms

In order to realize the Hilbert transform of a discrete signal, it can be processed using the Discrete Fourier Transform (DFT). The principle is as follows:

1. DFT is performed on the discrete signal $\theta(n)$ to obtain $F(k)$, where $k = 0,1,\cdots,N-1$.

2. Let $G(k) = \begin{cases} F(k) & k = 0 \\ 2F(k) & k = 1,2,\cdots,N/2-1 \\ 0 & k = N/2,\cdots,N-1 \end{cases}$.

3. Discrete Fourier inverse transform (IDFT) is applied to $G(k)$ to obtain the analytic signal $\boldsymbol{\beta}(n)$ for $\theta(n)$.

4. The Hilbert transform of $\theta(n)$ is $\tilde{\theta}(n) = \mathrm{IDFT}\{-\mathrm{j}[G(k) - F(k)]\}$.

3.1.3 Computational principles

The normalized rotational inertia measurement model can be expressed as:

$$\ddot{\theta} + \sum_{j=0}^{n} c_j \,|\,\dot{\theta}\,|^j \cdot \mathrm{sgn}(\dot{\theta}) + \sum_{i=1}^{m} k_i \,|\,\theta\,|^i \cdot \mathrm{sgn}(\theta) = 0 \tag{11}$$

where n is the highest order of angular velocity and m is the highest order of angular displacement.

For ease of analysis, Eq. (11) can also be expressed as:

$$\ddot{\theta} + 2h_0(t)\dot{\theta} + \omega_0^2(t)\theta = 0 \tag{12}$$

where $h_0(t)$ is the instantaneous damping coefficient and $\omega_0(t)$ is the instantaneous undamped intrinsic frequency.

Assume that $h_0(t), \omega_0(t)$ is a low-pass signal and $\theta(t)$ is a high-pass signal, and that the spectra of $h_0(t), \omega_0(t)$ and $\theta(t)$ do not overlap in the frequency band.

Do the Hilbert transform on both sides of Eq. (12) and multiply by j, then add with Eq. (12) to obtain:

$$\ddot{\boldsymbol{\beta}} + 2h_0(t)\dot{\boldsymbol{\beta}} + \omega_0^2(t)\boldsymbol{\beta} = 0 \tag{13}$$

Derivation on both sides of Eq. (13) yields:

$$\dot{\boldsymbol{\beta}} = \boldsymbol{\beta}\left[\frac{\dot{A}}{A} + j\omega\right] \tag{14}$$

$$\ddot{\boldsymbol{\beta}} = \boldsymbol{\beta}\left[\frac{\ddot{A}}{A} - \omega^2 + 2j\frac{\dot{A}\omega}{A} + j\dot{\omega}\right] \tag{15}$$

Substituting Eq. (14) and Eq. (15) into Eq. (13) yields:

$$\boldsymbol{\beta}\left[\frac{\ddot{A}}{A}-\omega^2+\omega_0^2+2h_0\frac{\dot{A}}{A}+j\left(2\frac{\dot{A}}{A}\omega+\dot{\omega}+2h_0\omega\right)\right]=0 \tag{16}$$

Let the real and imaginary parts of equation (16) be zero, the instantaneous undamped intrinsic frequency $\omega_0(t)$ and the instantaneous damping coefficient $h_0(t)$ of the torsional pendulum motion can be obtained after finishing the calculation:

$$\omega_0(t)=\left[\omega^2-\frac{\ddot{A}}{A}+\frac{2\dot{A}^2}{A^2}+\frac{\dot{A}\dot{\omega}}{A\omega}\right]^{\frac{1}{2}} \tag{17}$$

$$h_0(t)=-\frac{\dot{A}}{A}-\frac{\dot{\omega}}{2\omega} \tag{18}$$

Meanwhile, the relationship between the instantaneous undamped intrinsic frequency, instantaneous damping coefficient and Eq. (11) can be expressed as follows:

$$\omega_0(A)=\left[\sum_{i=1}^{m}\frac{2}{\sqrt{\pi}}\frac{\Gamma\left(\frac{i}{2}+1\right)}{\Gamma\left(\frac{i+1}{2}+1\right)}k_i\cdot A^{i-1}(t)\right]^{\frac{1}{2}} \tag{19}$$

$$h_0(A\omega)=\sum_{j=0}^{n}\frac{1}{\sqrt{\pi}}\frac{\Gamma\left(\frac{j}{2}+1\right)}{\Gamma\left(\frac{j+1}{2}+1\right)}c_j\cdot[A(t)\omega(t)]^{j-1} \tag{20}$$

For the rotational inertia measurement model I, the relationship between the instantaneous undamped intrinsic frequency $\omega_0(t)$, the instantaneous damping coefficient $h_0(t)$, and the normalized measurement model can be obtained according to Eqs. (19) and (20):

$$\begin{cases}\omega_0(A)=\left[k_1+\frac{3}{4}k_3A^2(t)\right]^{\frac{1}{2}}\\ h_0(A\omega)=\frac{c_1}{2}+\frac{4c_2}{3\pi}A\omega\end{cases} \tag{21}$$

For the rotational inertia measurement model I, the relationship between the instantaneous undamped intrinsic frequency $\omega_0(t)$, the instantaneous damping coefficient $h_0(t)$, and the normalized measurement model can be obtained according to Eqs. (19) and (20):

$$\begin{cases} \omega_0(A) = \left[k_1 + \dfrac{3}{4} k_3 A^2(t) \right]^{\frac{1}{2}} \\ h_0(A\omega) = \dfrac{c_1}{2} + \dfrac{4c_2}{3\pi} A\omega \end{cases} \tag{22}$$

According to Eq. (19) and Eq. (20), the normalized measurement model parameters can be calculated by using the method of least-squares curve fitting, and finally the moment of inertia of the measured object can be found out according to the stiffness coefficient of the torsion bar K_1:

$$J = \frac{K_1}{k_1} \tag{23}$$

For the time-varying rotational inertia measurement model, the relationship between the time-varying rotational inertia and the instantaneous undamped intrinsic frequency:

$$J(\tau) = \frac{K_1 + K_3\theta^2}{\omega_0^2} \tag{24}$$

The detailed procedure for determining rotational inertia with the Hilbert-transform-based approach is presented in Fig. 2. To begin with, the angular-displacement waveform of the measured object is processed through the Hilbert transform, and the corresponding analytic signal is obtained. Subsequently, the instantaneous amplitude, instantaneous phase, and instantaneous angular frequency of the angular-displacement waveform are derived. On this basis, the undamped natural frequency and damping coefficient of the torsion-pendulum vibration are determined according to Eqs. (17) and (18). The relevant parameters required for rotational inertia measurement are then identified from Eqs. (19) and (20) by applying a least-squares curve-fitting procedure. In the final step, the stiffness coefficient of the torsion bar is used to calculate the moment of inertia of the measured object.

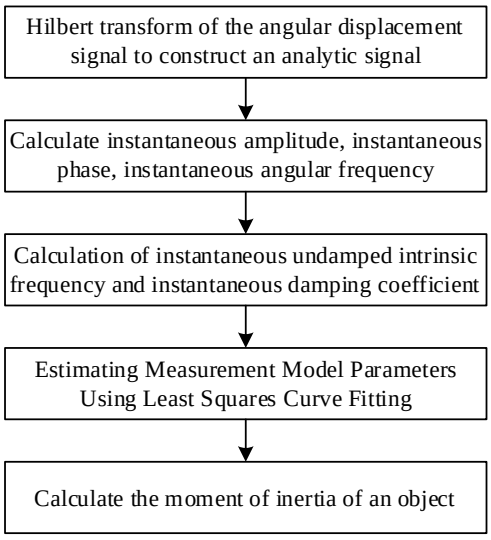

Figure 2: Calculation method of moment of inertia based on Hilbert transform

3.2 Empirical model decomposition

Before calculating the rotational inertia of the target object, it is essential to find out the instantaneous angular frequency of the torsional vibration of the target object. In order to derive the instantaneous angular frequency, it is important to consider that the wave analyzed must have only one component of angular frequency at each time point. That means, single component waves have unique angular frequency at each time point while multiple component waves do not have such unique angular frequency at each time point. Therefore, it is important to decompose the multiple component wave into multiple single component waves using suitable methods. The empirical mode decomposition method will enable us to decompose the multiple component wave into multiple single component waves, called intrinsic mode functions that represent angular-frequency information physically. Thus, before using the Hilbert transform method to calculate rotational inertia, it is important to use the EMD to know whether the angular displacement wave is a single component wave or not.

(1) Identify all local maxima and minima of the original waveform $\theta(t)$. Then, apply a cubic spline to connect all local maxima and generate the upper envelope, and use another cubic spline to connect all local minima so as to obtain the lower envelope.

(2) Take the average of the upper and lower envelopes as $m_1(t)$:

$$h_1(t) = \theta(t) - m_1(t) \tag{25}$$

(2) Determine whether $h_1(t)$ is an IMF component or not; ideally, $h_1(t)$ is an IMF component.

(3) If $h_1(t)$ does not satisfy the criterion of IMF, repeat the steps of (1) and (2) with $h_1(t)$ as the original signal:

$$h_{11}(t) = h_1(t) - m_{11}(t) \tag{26}$$

where $m_{11}(t)$ is the average of the upper and lower envelopes of the signal $h_1(t)$.

(4) If $h_{11}(t)$ does not satisfy the criteria of IMF, then $h_{11}(t)$ is used as the original signal and the steps k of (1) and (2) are repeated k times until $h_{1k}(t)$ satisfies the criteria of IMF:

$$c_1 = h_{1k}(t) = h_{1(k-1)}(t) - m_{1k}(t) \tag{27}$$

(5) Separate the c_1 component from the signal $\theta(t)$ and what remains is the new signal. Then, steps (1) to (4) are repeated to obtain $\mathrm{IMF_i}$ and the residual function:

$$\theta(t) = \sum_{i=1}^{n} c_i + r_n \tag{28}$$

In order to keep the number of decompositions of the signal within reasonable limits, the standard deviation of the neighboring signals $h_{1k}(t)$ and $h_{1(k-1)}(t)$ can be used as a termination criterion for the decomposition process:

$$SD = \sum_{t=0}^{T} \left[\frac{|h_{1(k-1)})(t) - h_{1k}(t)|^2}{h_{1(k-1)}^2(t)} \right] \tag{29}$$

Practical results show that the decomposition results satisfy the condition when SD is between 0.2 and 0.3.

Suppose the simulated signal $\theta(t)$ consists of several single-component signals as shown in the following equation:

$$\theta(t) = 10\sin\left(2\pi f_1 t\right) + 5\sin\left(2\pi f_2 t\right) \tag{30}$$

where $f_1 = 10\text{Hz}$, $f_2 = 100\text{Hz}$ and the sampling frequency $f_s = 1000\text{Hz}$.

4 Measurement experiment of rotational inertia and mechanical error analysis

4.1 Experimental equipment for rotational inertia measurement

The reference components adopted in this system are standard masses. Different mass combinations are selected as the objects under test, and the rotational inertia to be identified corresponds to the inertia value of these combined masses about the torsion axis. The theoretical values of mass and inertia for the different standard masses were calibrated by the relevant metrological authority, as listed in Table 1, where m denotes the mass of the weights and J represents the theoretical inertia value of the weights with respect to the central axis.

Table 1: The Mass and Moment of Inertia of a Weight

Weight Number	F0	F1	F2	F3	F4
m/(kg)	18.8143	19.9132	18.8452	19.8421	19.8469
J/(kg.m²)	0.0987	0.0987	0.0985	0.0982	0.0982
Weight Number	F5	F6	F7	F8	F9
m/(kg)	19.8645	19.0985	19.8372	19.8862	19.8029
J/(kg.m²)	0.0983	0.0897	0.0985	0.0986	0.0981

The schematic structure of the bar carrier is shown in Fig. 3, and the distance relationship of each positioning seat is shown in Table 2.

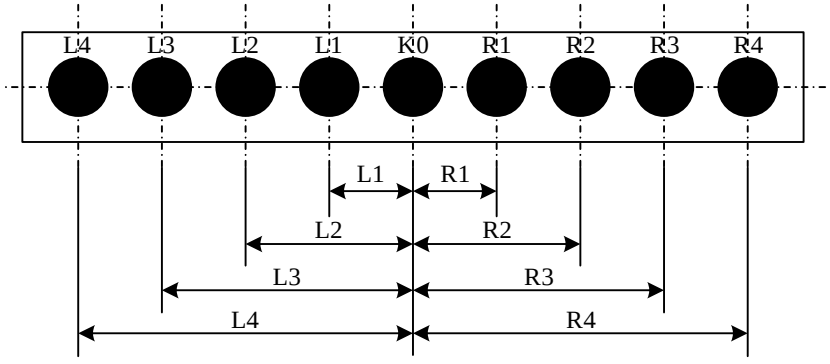

Figure 3: Schematic diagram of the structure of the bar-shaped stage

Table 2: Distance Relationship of Each Positioning Seat on the Bar-shaped Stage

Distance symbol	L1	L2	L3	L4
Calibration value(mm)	300.457	602.182	904.374	1204.564
Distance symbol	R1	R2	R3	R4
Calibration value(mm)	300.437	603.423	905.181	1204.173

4.2 System calibration experiment

The torsional stiffness coefficient K of the torsion bar and the unloaded rotational inertia J0 of the torsion-pendulum table under real operating conditions must first be determined, and this stage constitutes system calibration. An unloaded measurement is therefore performed to obtain the instantaneous amplitude and instantaneous angular frequency of the principal component of angular displacement under the first no-load condition, as illustrated in Fig. 4 and Fig. 5.

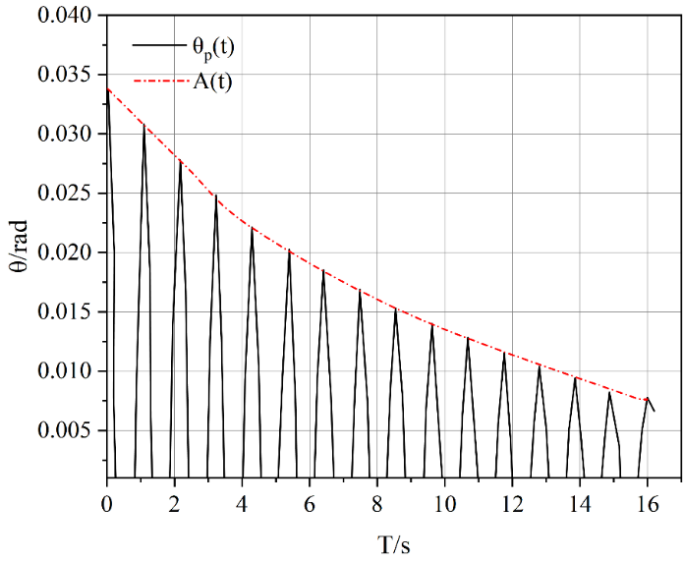

Figure 4: Instantaneous amplitude under no-load condition

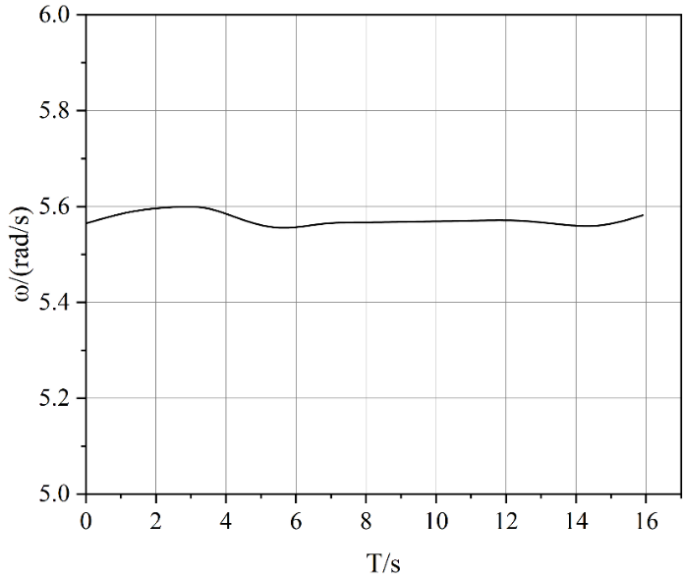

Figure 5: Instantaneous Frequency under No-load Condition

The instantaneous damping coefficient together with the instantaneous undamped natural frequency of the torsion-pendulum system derived from the solution are presented in Figs. 6 and 7. Under the no-load condition, the instantaneous damping coefficient decreases to 0.077, while the intrinsic frequency decreases to 0.038.

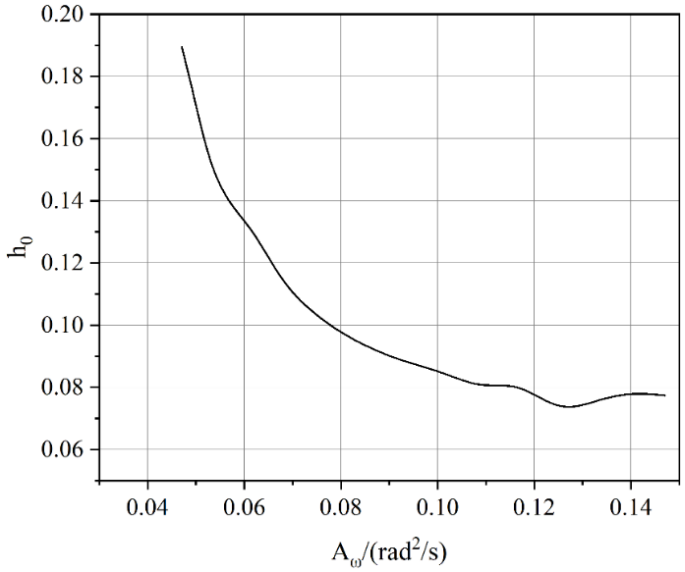

Figure 6: Instantaneous damping coefficient under no-load condition

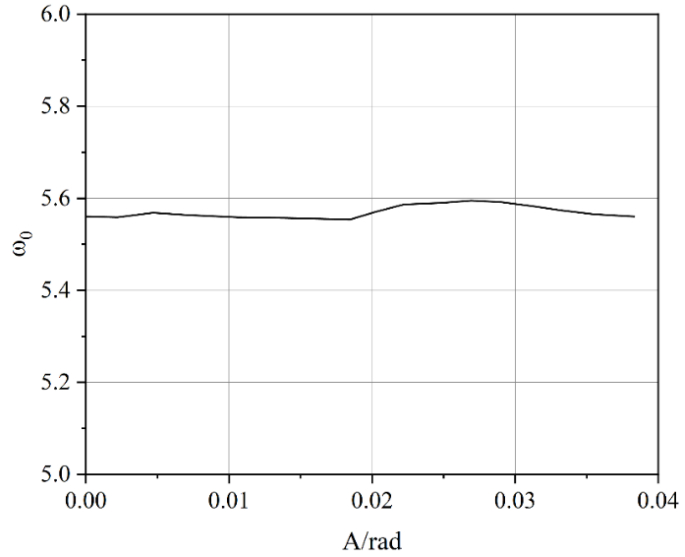

Figure 7: Instantaneous undamped natural frequency at no load

The normalized model physical parameter estimates are obtained by fitting the transient modal parameter curves of Figures 6 and 7 using the least squares method as shown in Table 3.

Table 3: Estimation of normalized parameters under no-load condition

Normalized parameter	$f/(s^{-2})$	$c/(s^{-1})$	$k/(rad^{-1}.s^{-2})$
Estimated value	0.00249	0.150926	32.1124

In order to verify the accuracy of the estimation of the physical parameters of the normalized model, the angular displacement estimation results are solved by Pearson correlation coefficient

with the real angular displacement. Among them, the angular displacement estimation results are solved by using the fourth-order Longe-Kuta method, setting the sampling frequency as 300 Hz, the initial torsion angle as 0.0351 rad, which is the same as the torsion angle of the real angular displacement, and the initial angular velocity is zero. The real angular displacement signal and the estimation result are shown in Fig. 8, where $\theta(t)$ is the real value of the angular displacement and $\theta_{est}(t)$ indicates the estimated value of the angular displacement, and the figure has a good fitting accuracy.

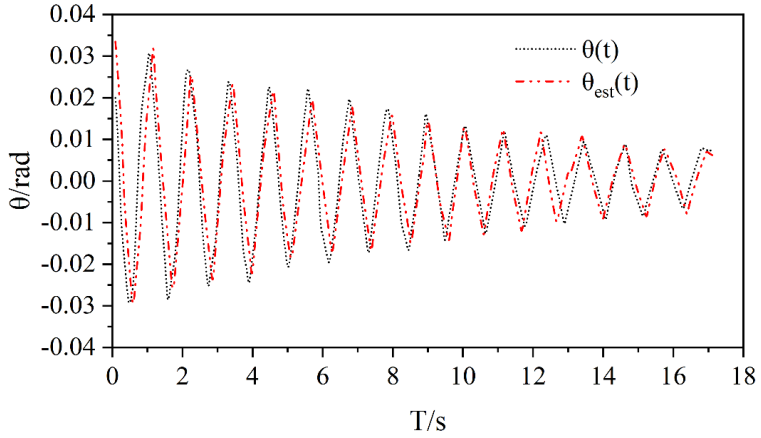

Figure 8: Comparison of Real Value and Estimated Value of Angular Displacement

The Pearson correlation coefficient ρ is expressed as:

$$\rho = \frac{E\left(\theta \cdot \theta_{est}\right) - E(\theta)E\left(\theta_{est}\right)}{\sqrt{E\left(\theta^2\right) - E^2(\theta)} \cdot \sqrt{E\left({\theta_{est}}^2\right) - E^2\left(\theta_{est}\right)}} \tag{31}$$

where $E()$ denotes the mathematical expectation.

During system calibration, three sets of masses with different combinations were placed symmetrically on the torsion bar, and the result for each combination was taken as the mean of three repeated measurements. The corresponding outcomes for the standard components are given in Table 4, in which J_{tr} denotes the theoretical rotational inertia of different mass combinations about the axis of the torsion pendulum. The masses of combinations 2 and 3 are 41.7109 kg and 41.7042 kg, respectively, while their rotational inertia values are 59.2681 kg·m² and 59.2574 kg·m², respectively. These values are very close to each other and the associated errors are relatively small, indicating that the experiment is stable. The difference in the masses of the combinations therefore exerts only a limited influence on the measurement results.

Table 4: Measurement results for standard parts

Combination number	m/(kg)	J_{tr} /(kg.m²)	k/(rad^{-1}.s^{-2})
1	81.2743	116.5732	13.6738
2	41.7109	59.2681	19.1075
3	41.7042	59.2574	19.1152

4.3 Product Measurement Results and Analysis

4.3.1 Measurement results

The combination of weights is shown in Figure 9. According to the relationship between the mass of each weight, the rotational inertia and the distance between each base of the bar carrier, the theoretical value of the rotational inertia of the product $J_C = 138.2143\text{kg}\cdot\text{m}^2$ is obtained by using calculations.

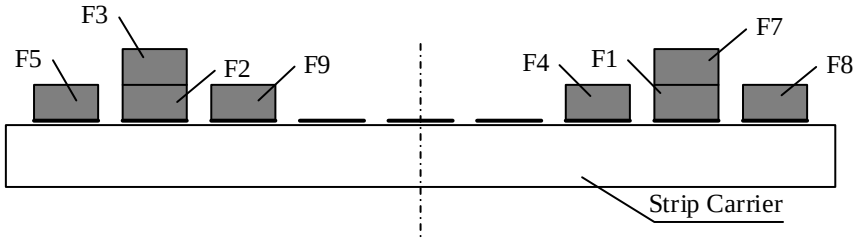

Figure 9: Diagram of weight combinations

Setting the sampling frequency as 300Hz, the angular displacement signal $\theta(t)$ is acquired, and it is processed to extract the main component, and the EMD processing results are obtained as shown in Fig. 10. From the figure, it can be seen that IMF_1 is high-frequency noise, IMF_2 is basically the same as $\theta(t)$, and according to the calculation of energy, we get that IMF_2 accounts for 99.4% of the total, and IMF_2 is extracted as the main component of the angular displacement.

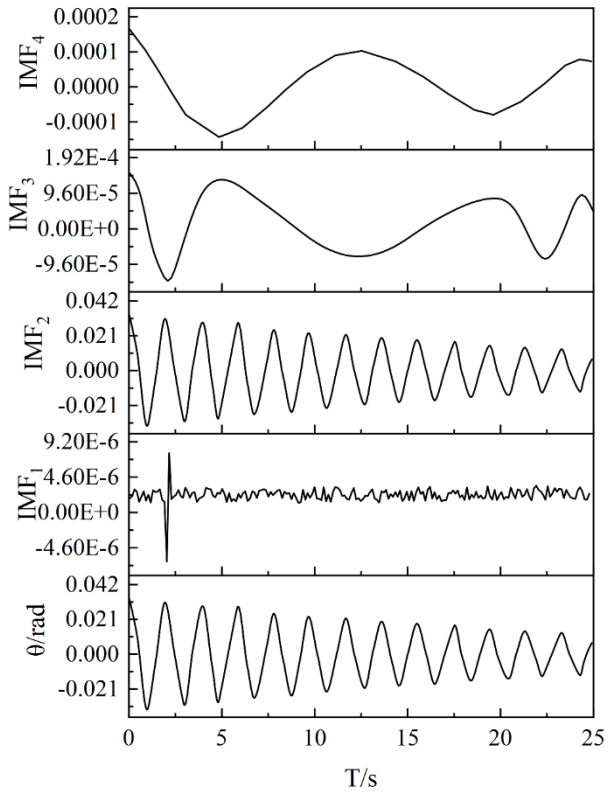

Figure 10: EMD processing results of angular displacement under product measurement conditions

The improved EE approach is employed to derive the instantaneous amplitude and instantaneous angular frequency of the principal component $\theta_p(t)$ after which the instantaneous undamped natural frequency is determined and the physical parameters of the normalized model are estimated through least-squares fitting according to Eq. (6). The identified values of the instantaneous undamped natural frequency together with the fitting outcomes are presented in Fig. 11, indicating that the fitting deviation is relatively small.

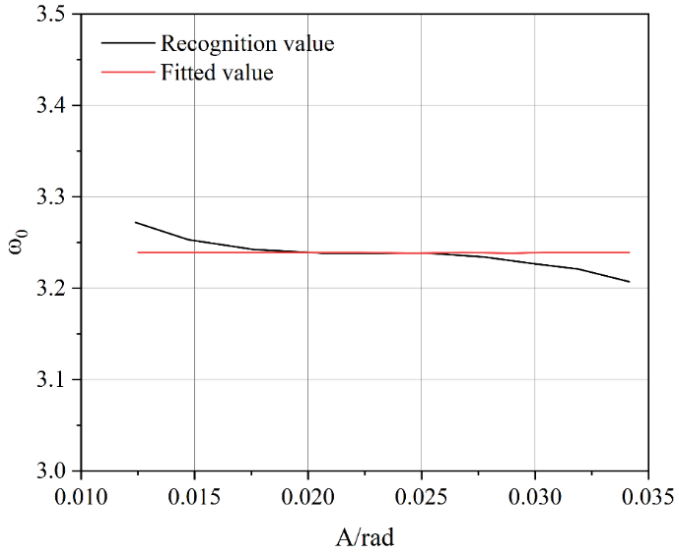

Figure 11: Identification and fitting results of instantaneous undamped natural frequency

Various weights were used in the rotation inertia experiment, and their respective results have been provided in Table 5. The last column, which indicates the relative error, clearly indicates that the rotational inertia error of the measured objects meets the prescribed criteria.

Table 5: Product measurement results

Combination number	m/(kg)	J_{tr}/(kg.m²)	k/(rad^{-1}.s^{-2})	J_{mea}/(kg.m²)	δ/%
1	41.7474	59.3838	19.0457	59.4181	0.08
2	81.4901	91.755	15.6022	91.6	-0.15
3	120.9934	131.0381	12.9108	130.9151	-0.13
4	121.1494	124.0582	13.2989	124.0886	0.04
5	160.705	134.8052	12.7099	134.6434	-0.14
6	160.7361	188.4215	10.4663	188.3229	-0.07
7	160.7855	138.521	12.4994	138.7031	0.15
8	160.7855	163.4808	11.3698	163.6095	0.07
9	186.8135	172.906	11.0102	173.1238	0.15
10	206.6392	174.7865	10.9279	175.0708	0.18

4.3.2 Comparison of measurement results

Following the same measurement steps, the system was calibrated using the rotational inertia calculation algorithm based on the Hilbert transform to obtain the stiffness coefficient of the torsion bar K=2214.1342N·m·rad^{-1} and the no-load rotational inertia J_0 = 71.0382kg-m², and the product measurement results are shown in Table 6.

Table 6: Product measurement results(MR_{tr} =24mm)

Combination number	m/(kg)	J_{tr}/(kg.m²)	k/(rad^{-1}.s^{-2})	J_{mea}/(kg.m²)	δ/%
1	41.7474	59.3838	19.0972	59.3409	-0.09
2	81.4901	91.755	15.6392	91.5887	-0.22
3	120.9934	131.0381	12.9407	130.9335	-0.011
4	121.1494	124.0582	13.3364	123.9906	0.07
5	160.705	134.8052	12.7441	134.5734	-0.19
6	160.7361	188.4215	10.4848	188.5315	0.08
7	160.7855	138.521	12.5395	138.5059	-0.02
8	160.7855	163.4808	11.3959	163.6449	0.11
9	186.8135	172.906	11.0216	173.2595	0.22
10	206.6392	174.7865	10.9697	174.6561	-0.09

The results for the system calibration change depending on whether the stroke of the piston rod exceeds that of a smaller stroke. However, as can be seen from Tables 5 and 6, the rotational inertia of the objects tested stays within 0.5%, thus meeting the specifications. When the stroke of the piston rod increases, it results in an increased initial angle of twist, allowing the torsion bar to remain twisted for a longer duration. This allows more data on the angular displacement over torsional cycles to be collected for the calculation of inertia.

The standardized components were also measured by means of the periodic approach, and the corresponding results are reported in Table 7, where ζ denotes the system damping ratio obtained through calculation, and T denotes the torsion-pendulum period, defined as the mean value of three period measurements for each combination. The period is identified by extracting the intersection points between the angular-displacement curves and the time axis. Under no-load conditions, the system damping ratio is ζ_0=0.019, and the torsional period T_0=1.1287s.

Table 7: Measurement results for standard parts using the periodic method

Combination number	m/(kg)	J_{tr}/(kg.m²)	ζ	T/(s)
1	80.2573	116.6183	0.0115	1.8542
2	41.3872	59.3375	0.0147	1.5438
3	41.3816	59.3284	0.0139	1.5454

The torsional stiffness coefficient of the torsion bar and the unloaded torsion-bar moment of inertia were calculated as K=2207.2544N·m·rad^{-1} and J_0=71.4583kg·m² respectively. The results for the moment-of-inertia calculation of different weight combinations using the periodic approach are listed in Table 8. As the mass increases and the moment of inertia becomes larger, the torsional period lengthens, the number of observable torsional cycles decreases, and the relative error associated with the periodic approach correspondingly grows.

Table 8: Periodic method product measurement results

Combination number	m/(kg)	J_{tr}/(kg.m²)	δ	T/(s)	J_{mea}/(kg.m²)	δ/%
1	41.7474	59.3838	0.0192	1.6333	59.516	0.22
2	81.4901	91.755	0.0198	1.8147	91.6473	-0.13
3	120.9934	131.0381	0.0207	2.0153	131.3837	0.264
4	121.1494	124.0582	0.0189	1.9786	123.7852	-0.22
5	160.705	134.8052	0.0214	2.0326	135.0139	0.15
6	160.7361	188.4215	0.0205	2.2741	189.1824	0.40
7	160.7855	138.521	0.0189	2.0518	139.0995	0.42
8	160.7855	163.4808	0.0195	2.1659	164.1298	0.40
9	186.8135	172.906	0.0196	2.2071	173.5197	0.35
10	206.6392	174.7865	0.0197	2.216	175.572	0.45

A comparison between the errors made in estimating the periodic and Hilbert transform methods is shown in Figure 12 below. It can be seen from the figure that the error involved in estimating the rotational inertia using the Hilbert transform is lower compared to that made while doing the same process using the periodic method. It shows that the Hilbert transform method performs better when it comes to estimating the rotational inertia compared to the periodic method, especially for objects having a relatively high mass or moment of inertia.

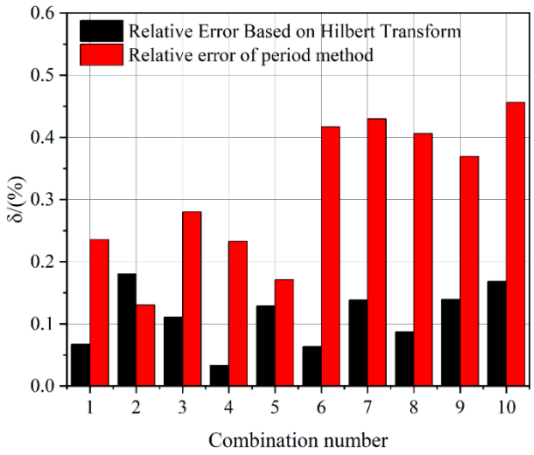

Figure 12: Comparison of Relative Errors of Rotational Inertia

4.3.3 Mechanical error analysis

1. Error analysis caused by inaccurate period measurement

In the vibration compound pendulum system, the rotational inertia measurement value is proportional to the square of the swing period, therefore, the measurement accuracy of the swing period will have a direct impact on the testing accuracy of the rotational inertia, the device uses the square wave signal output from the optoelectronic sensor is converted into a voltage signal through the signal processing circuit, so as to calculate the swing period, assuming that the measurement error of the swing period is ΔT, the resultant Rotational inertia test error is:

$$\Delta 1 = \frac{\Delta J}{J} \times 100\% = \frac{2\Delta T}{T} \times 100\% \tag{32}$$

In actual measurement, the minimum swing period is 2.8764s, the photoelectric sensor itself period measurement error is 0.1ms, then due to the period measurement error caused by the rotational inertia test error $\Delta 1$=0.0042%

2. Elastic release mechanism error

The test by releasing the positioning pin, so that the torsion pendulum disk with the elastic body swing, to ensure that the elastic body each time the starting position of the swing is the same, due to the previous equipment used in the positioning pin is a mechanical structure, and the angle of the locking device between the existence of a certain amount of friction between the different testers, each time to apply a different force, resulting in a fast release and the slow release of the effect is not the same at all, so that the instrument each time to measure the swing cycle value is very large difference. The instrument's swing period value varies a lot every time it is measured.

3. Radial offset error of the measured object

The accuracy of the center-of-mass measurement has a significant impact on the measurement of the inertia of the projectile, because according to the traditional measurement method, when measuring its equatorial moment of inertia, it is required that the axis of rotation of the projectile absolutely passes through its center of mass. If there is an error in the measurement of the center of mass or the placement of the projectile is inaccurate, then according to the method of measuring the equatorial moment of inertia, the projectile is not rotating around the true center of mass line, which results in the transfer of error and causes a larger error. According to the Parallel Axis Theorem, it can be seen that if the axis of rotation deviates from its center of mass line Δz, an error of $m\Delta z^2$ will result for a projectile with a mass M:

$$\delta_2 = \frac{\Delta J}{J} = \frac{m\Delta z^2}{J} \tag{33}$$

4. Error of the rotation axis of the measured object not being perpendicular to the horizontal plane

Due to the irregularity in the bottom surface, which is a result of the geometrical construction of the measuring sling and pointer, as well as operational reasons, tilting of the tested body upon mounting to the pallet will occur. The tilting of the tested body causes displacement of the rotation axis relative to the axis of the tested body. Moreover, during the measurement of either the polar or equatorial moment of inertia, the axis of the tested body may not maintain its horizontal position.

5. The effect of different temperatures on the torsion bar error

As the temperature increases, the hardness and strength gradually decrease. This is mainly because when tempering at temperatures above 350°C, the quenched martensite gradually decomposes, but the α-phase still maintains a needle-like shape, and the ε-carbides and x-carbides formed before have disappeared at this time and transformed into Θ-carbides. As the temperature increases, the hardness and strength gradually decrease, while the plasticity and toughness improve slightly. The change in hardness and strength of the torsion bar due to temperature increases the uncertainty and therefore leads to measurement errors.

5 Research on error compensation algorithm of rotational inertia measurement

Different temperature levels of the torsion bar result in different stiffness coefficients and hence

large differences in the measured value of the rotational inertia. In order to overcome the problem that different temperatures of the torsion bar affect the measurement of rotational inertia, it is necessary to have a suitable compensation approach for the stiffness coefficient in terms of temperature. Based on this concept, a compensation method for the stiffness coefficient and rotational inertia in terms of temperature is established.

5.1 Compensation principle based on the least squares method

The compensation formula is a way of numerically correcting the measurement error, and the key to deriving the formula is the fitting of the relationship function between the damping ratio and the relative error. The so-called fitting refers to the selection of appropriate curves to portray or describe the functional relationship between the coordinates of discrete points on the plane of a data processing method, there are a variety of data constraints and limiting criteria, is mathematical approximation and optimization. At present, the main fitting methods are mean value method, difference difference quotient method, least squares method, etc. The more commonly used is the least squares fitting method.

Least squares (also known as least square) fitting is widely used in many fields of science and engineering technology, and is a more commonly used data processing optimization technique. It should be noted that by using least squares, one can achieve such an equation of the curve that will provide minimal deviations from the points, taking into account all the coordinates. Within the context of least squares fitting, the task of data optimization can be solved. In essence, data processed according to the least squares conditions can effectively reduce random errors, thereby increasing the confidence, stability, and accuracy of the results obtained.

The principle of fitting the linear equation using the least squares principle is as follows.

The general equation of the linear equation is given by:

$$y = ax + b \tag{34}$$

Its residual sum of squares equation is:

$$Q = \sum_{i=1}^{m} \left[y_i - (ax + b) \right]^2 \tag{35}$$

By definition, the parameters a, b are the ones that produce the smallest sum of squares of the distances of the observed values from the predicted line as per the least squares method. The condition $\frac{\partial Q}{\partial a} = 0, \frac{\partial Q}{\partial b} = 0$ is satisfied when Q has a minimum value. There is:

$$\begin{cases} bN + a\sum_{i=1}^{m} x_i = \sum_{i=1}^{m} y_i \\ b\sum_{i=1}^{m} x_i + a\sum_{i=1}^{m} x_i^2 = \sum_{i=1}^{m} x_i y_i \end{cases} \tag{36}$$

Further derive an expression for the coefficients a, b of the linear equation, viz:

$$\begin{cases} a = \dfrac{\sum_{i=1}^{m} x_i \sum_{i=1}^{m} y_i - n\sum_{i=1}^{m} x_i y_i}{\left(\sum_{i=1}^{m} x_i\right)^2 - n\sum_{i=1}^{m} x_i^2} \\ b = \dfrac{\sum_{i=1}^{m} x_i y_i \sum_{i=1}^{m} x_i - \sum_{i=1}^{m} y_i \sum_{i=1}^{m} x_i^2}{\left(\sum_{i=1}^{m} x_i\right)^2 - n\sum_{i=1}^{m} x_i^2} \end{cases} \tag{37}$$

5.2 Derivation of the compensation algorithm

The torsion bar stiffness coefficients obtained from the temperature compensation experiments and the corresponding mechanical data were subjected to least squares curve fitting, and the coefficients of the fitted linear equations were derived by fitting the data using the cftool toolbox in matlab to treat each different load case as a set of data, which was divided into a total of four sets of data for the no-load case, two-weights-load case, four-weights-load case, and six-weights-load case. The results of fitting these data are shown in Figure 13. The results of the parameters and of the fitted linear equations are shown in Table 9.

In all of the curves that have been fitted, the value of R is greater than 0.99. R has a range of values between 0 and 1, and the closer it gets to 1, the more likely the result of the fitting process becomes; thus, the lines presented below are very likely results of the fitting process.

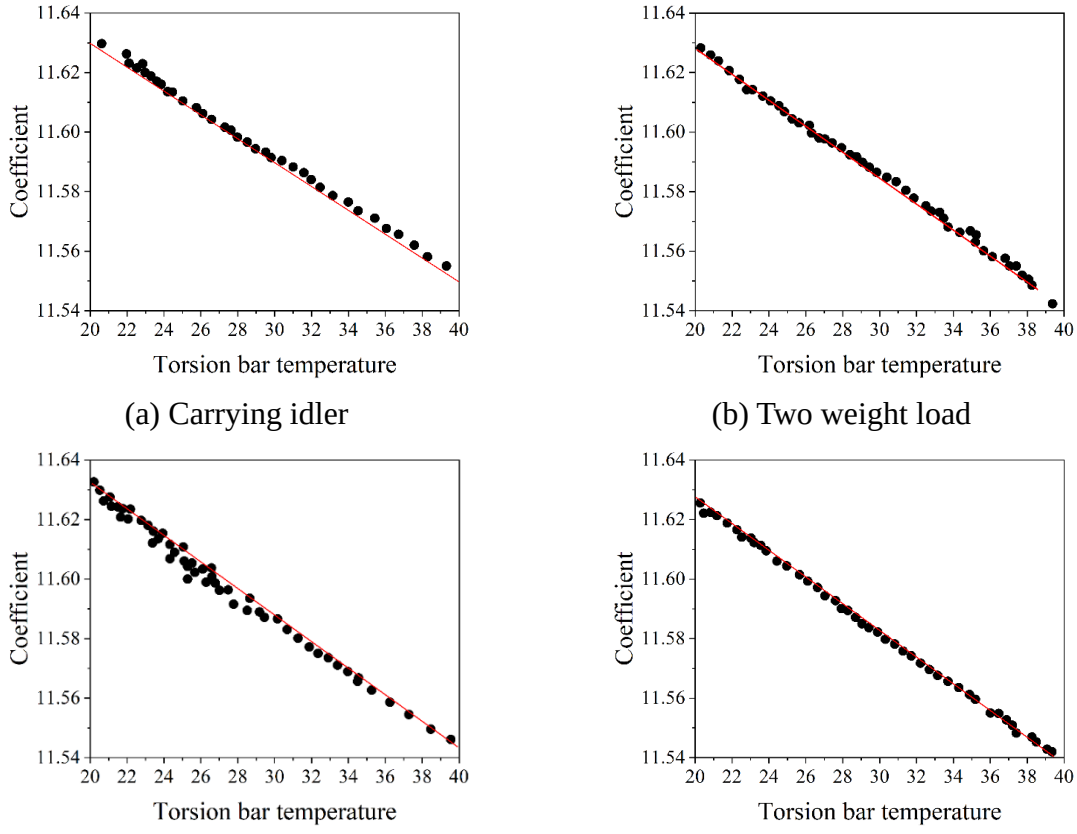

(a) Carrying idler (b) Two weight load

(c) Four weight load (d) Hexagonal silicon code load

Figure 13: Fitting results of torsion bar stiffness coefficient with torsion bar mechanical change

Table 9: Fitting results of torsion bar stiffness coefficient with torsion bar mechanical change

Order number K	Load condition	J_{tr} kg.m²)	a_k (10^{-3})	b_k (N.m/rad)
1	Carrying idler	95.213	-5.000	12.831
2	Two weight	59.083	-5.039	12.831
3	Four weights	114.072	-4.573	12.802
4	Six weights	146.618	-4.649	12.802
5	Average value	-	-4.773	12.811

The results for the parameters a and b of the equations fitted to the four sets of data were averaged and used as the final result of the fit:

$$A = -4.773\times10^{-3}T_{emp} + 12.811 \tag{38}$$

During actual usage, the stiffness of the torsion bar is adjusted before each measurement, and this adjustment corrects for part of the measurement error, including the dampening effect caused by the rotary table. The following is a general equation that can be used to calculate the temperature correction factor for the torsion bar stiffness coefficient based on their correlation as described in Chapter II.

$$A = -4.773\times10^{-3}\left(T_{emp} - T_{emp0}\right) + A_0 \tag{39}$$

where A_0 - calibrated torsion bar stiffness factor ($\mathrm{N\cdot m/rad}$).

T_{emp} - real-time temperature of the torsion bar during the measurement.

T_{emp0} - temperature during system calibration.

Temperature compensation algorithm for rotational inertia measurement:

$$J = \left[-4.773\times10^{-3}\left(T_{emp} - T_{emp0}\right) + A_0\right]T^2 - J_0 \tag{40}$$

where J_0 - the calibrated unloaded moment of inertia of the air-bearing rotary table ($\mathrm{kg\cdot m^2}$).

T - measured torsional period (s) of the air-bearing rotary table.

5.3 Validation of the compensation algorithm

Therefore, the objective of validating the temperature compensation algorithm lies in determining the extent to which the accuracy of measuring rotational inertia under temperature fluctuations of the torsion bar can be significantly improved through applying compensation. Indeed, the validation of the temperature compensation algorithm is supposed to reveal both the viability of the new algorithm and its capacity to compensate for temperature effects by analyzing the measurements of rotational inertia prior to and after temperature compensation. In other words, the focus of the validation process is placed on testing the measurement results before and after compensation.

By comparing the relative errors δ_M and δ_C of rotational-inertia measurement before and after temperature compensation, the feasibility and effectiveness of the compensation algorithm can be confirmed. The relative error δ is calculated by the following formula:

The relative error δ is calculated by the formula:

$$\delta = \frac{J - J_{TH}}{J_{TH}} \times 100\% \tag{41}$$

where J_{TH} - theoretical value of the moment of inertia of the loaded standard weight ($\mathrm{kg \cdot m^2}$);

J - the measured value of the rotational inertia of the loaded standard weight ($\mathrm{kg \cdot m^2}$).

During the validation stage, the stiffness coefficient and the unloaded moment of inertia of the torsion bar were first calibrated, and the temperature of the torsion bar at the time of calibration was recorded. The calibrated outcomes are listed in Table 10.

Table 10: Calibration results of the rotational inertia measurement system

A_0(N.m/rad)	J_O(kg·m²)	T_{tem}(°C)
12.573	94.382	23.9

The stiffness constant determined experimentally from the torsion spring and air-bearing rotary table at 22.7°C and the moment of inertia of the no load condition, respectively, are utilized in the formulation of the temperature correction algorithm for the inertia measurement. This will help in determining the temperature correction algorithm for inertia in the validation of the current mechanical temperature algorithm.

$$J_C = \left[-4.773 \times 10^{-3} \left(T_{emp} - 23.9 \right) + 12.573 \right] T^2 - 94.382 \tag{42}$$

The torsion bar is heated by a small artificial sun until it stabilizes at about 40°C, and then the small artificial sun is removed to stop the heating process, and the temperature of the torsion bar will decrease continuously.In the measurement of the moment of inertia of four standard masses having a theoretical moment of inertia of $114.167\mathrm{kg \cdot m^2}$, the air-bearing rotary table was used. Using the compensation equation, temperature compensation was first carried out, and then using Equation (42), the rotational inertia of the four standard masses was calculated. The findings before and after the temperature compensation were compared to test the effectiveness of the temperature compensation method. To evaluate the effectiveness of the correction process, several rotational inertia values were measured, both with and without temperature compensation.

The inertia measurements before and after temperature compensation are processed, and some data are shown in Table 11.

Table 11: Results of the Mechanical Compensation of the Moment of Inertia of the Rod

T_{bm} /°C	J_M (kg.m²)	δ_M (%)	J_C (kg·m²)	δ_C (%)
40.2	115.542	1.204	114.202	0.031
38.4	115.4	1.08	114.183	0.014
37.1	115.296	0.989	114.159	0.007
35.3	115.167	0.876	114.159	0.007
33.6	115.049	0.773	114.151	0.014
32.7	114.995	0.725	114.158	0.008
31.9	114.917	0.657	114.139	0.025
30.6	114.861	0.608	114.164	0.003
29.3	114.795	0.55	114.19	0.02
27.5	114.726	0.49	114.238	0.062
26.5	114.653	0.426	114.233	0.058
25.6	114.614	0.392	114.239	0.063
23.9	114.558	0.342	114.219	0.046

In order to show more clearly the compensation effect of the derived temperature compensation algorithm, the results of all the experimental data processing are plotted using matlab. The comparison between the measured value of inertia of the four standard weights, the theoretical value and the value after temperature compensation of the measurement results is shown in Fig. 14, and the comparison between the relative error of measurement δ_C and δ_M before and after compensation is shown in Fig. 15.

By comparing Fig. 14 and Fig. 15, it can be clearly seen that the temperature compensation algorithm for rotational inertia measurement derived in this paper is very effective in compensating for temperature changes in rotational inertia measurement. The outcomes show that the developed approach successfully addresses the influence of temperature changes on the measurement of rotational inertia. With the temperature of the torsion bar changing between 20°C and 40°C, the maximum relative error in measurement without the application of temperature correction reaches 1%, greatly surpassing the ±0.1% accuracy required by the rotational-inertia measurement system. Using temperature correction, calculated using the experimental algorithm for temperature compensation, minimizes the relative error to below ±0.1%. Using the algorithm for temperature correction to counteract the effect of the temperature change of the torsion bar improves the accuracy of measurement at different temperatures of the torsion bar.

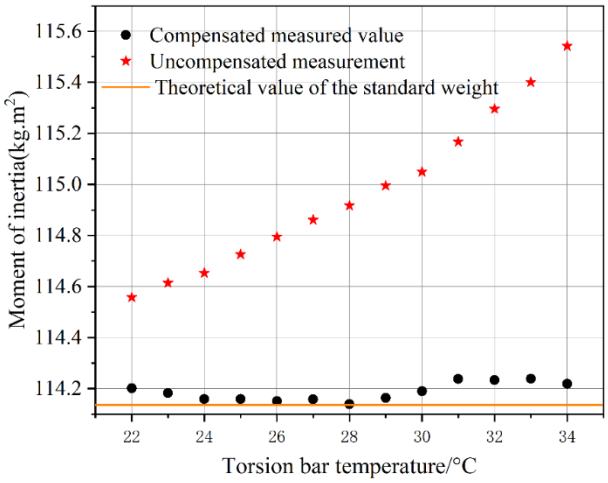

Figure 14: Comparison of the measurement results of the rotational inertia

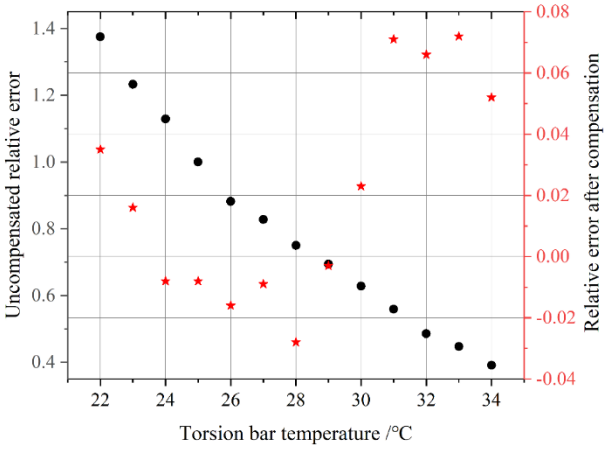

Figure 15: Comparative diagram of relative error before and after temperature compensation

6 Conclusion

Based on the functional relationship between rotational inertia and instantaneous undamped natural frequency of torsion pendulum oscillation, this paper introduces a method for calculating rotational inertia using Hilbert transform. An improved EE extraction technique is used to extract instantaneous features, and simulation results show that the proposed method can obtain more accurate measurements of rotational inertia than the traditional periodic analysis method, thus making it possible to use it in real rotational inertia measurements. Furthermore, the least squares criterion is used to verify the validity of the temperature compensation technique for rotational inertia measurement. Simulation results show that when the temperature of the torsion bar increases from about 20°C to 40°C, the relative error of rotational inertia measurement decreases from close to 1% to less than 0.1%.

Funding

This work was supported by Chongqing Research Institution Performance Incentive Guidance Special Project (Grant No. cstc2022jxjl60001).

About the Author

Yang Su was born in Jilin, China, in 1989. He obtained a master's degree from Changchun University of Science and Technology in China. He currently working at Chongqing Academy of Metrology and Quality Inspection. His main research direction is Mechanics and Optics metrology and testing technology.

Hang Xiu was born in Haerbin, Heilongjiang, China, in 1985. He obtained a master's degree from Jilin University in China. He currently working at Changchun University of Science and Technology Chongqing Research Institute. His main research direction is Engineering mechanics.

Lifang Wang was born in Chongqing, China, in 1983. She obtained a master's degree from Chongqing University in China. She currently working at Chongqing Academy of Metrology and Quality Inspection. Her main research direction is Mechanics metrology and testing technology.

Lei Cheng was born in Chongqing, China, in 1983. He obtained a master's degree from Chongqing University in China. He currently working at Chongqing Academy of Metrology and Quality Inspection. His main research direction is Mechanics metrology and testing technology.

Qi Qin was born in Chongqing, China, in 1988. She obtained a master's degree from Changchun University of Science and Technology in China. She currently working at Chongqing Institute of Engineering. Her main research direction is Computer application technology.

References

[1] Hinrichsen, P. F. (2022). A Simple Moment of Inertia Measurement. The Physics Teacher, 60(4), 292-295.

[2] Caprini, L., Gupta, R. K., & Löwen, H. (2022). Role of rotational inertia for collective phenomena in active matter. Physical Chemistry Chemical Physics, 24(40), 24910-24916.

[3] Klaus, L. (2017). Comparison of two experiments based on a physical and a torsion pendulum to determine the mass moment of inertia including measurement uncertainties. Measurement science review, 17(1), 9.

[4] Sziki, G. A., Szanto, A., & Adamko, E. (2024). Review of methods for determining the moment of inertia and friction torque of electric motors. Acta Polytechnica Hungarica, 21(4), 203-218.

[5] Zhong, Z., Wen, Q., Yan, J., & Pang, L. (2023). The Mean Moment of Inertia for Irregularly Shaped Phobos and Its Application to the Constraint for the Two-Layer Interior Structure for the Martian Moon. Remote Sensing, 15(12), 3162.

[6] Zhang, X. M., Wang, D. M., Li, J. Y., Shang, C. M., Xiong, J. X., & Xie, H. C. (2018). Deviation analysis of rotational inertia measurement based on torsion bar method. Vibroengineering Procedia, 21, 178-183.

[7] Thomson, M. (2023). DETERMINING MOMENT OF INERTIA USING A THREE-WIRE PENDULUM: AN IN-DEPTH TUTORIAL. Ayden International Journal of Basic and Applied Sciences, 11(2), 10-19.

[8] Morelli, E. A. (2022). Determining aircraft moments of inertia from flight test data. Journal of Guidance, Control, and Dynamics, 45(1), 4-14.

[9] Tang, S., Cao, Y., Shi, T., Yan, Y., & Xia, C. (2024). Online estimation of load torque and moment of inertia incorporating extended disturbance observer with trigger. IEEE Transactions on Power Electronics.

[10] Chen, Y., Zeng, Y., Li, H., Zhang, J., & Zhang, L. (2023). Research on the measurement technology of rotational inertia of rigid body based on the principles of monocular vision and torsion pendulum. Sensors, 23(10), 4787.

[11] Wang, Y. (2019, August). Research on moment of inertia measurement method. In IOP Conference Series: Materials Science and Engineering (Vol. 592, No. 1, p. 012078). IOP Publishing.

[12] Jung, S. (2020). A neural network technique of compensating for an inertia model error in a time-delayed controller for robot manipulators. International Journal of Control, Automation and Systems, 18(7), 1863-1871.

[13] Zhou, J., Liu, K., Zhang, Y., Chen, Y., Hu, W., Zhou, S., ... & Peng, X. (2025). Real-time Compensation of Dynamic Load Position Error with Pre-estimation of Mechanical Parameters for a Two-inertia Transmission System. IEEE Transactions on Energy Conversion.